UC Berkeley
UC Berkeley Previously Published Works

Title
Continental flood basalts drive Phanerozoic extinctions

Permalink
https://escholarship.org/uc/item/6890856q

Journal
Proceedings of the National Academy of Sciences of the United States of America, 119(38)

ISSN
0027-8424

Authors
Green, Theodore
Renne, Paul R
Keller, C Brenhin

Publication Date
2022-09-20

DOI
10.1073/pnas.2120441119

Peer reviewed

eScholarship.org Powered by the California Digital Library
University of California

PNAS RESEARCH ARTICLE | EARTH, ATMOSPHERIC, AND PLANETARY SCIENCES

Check for updates

Continental flood basalts drive Phanerozoic extinctions

Theodore Green[a,b,1], Paul R. Renne[c,d], and C. Brenhin Keller[a]

Edited by Andrew Knoll, Harvard University, Cambridge, MA; received November 9, 2021; accepted August 1, 2022

Refinements of the geological timescale driven by the increasing precision and accuracy of radiometric dating have revealed an apparent correlation between large igneous provinces (LIPs) and intervals of Phanerozoic faunal turnover that has been much discussed at a qualitative level. However, the extent to which such correlations are likely to occur by chance has yet to be quantitatively tested, and other kill mechanisms have been suggested for many mass extinctions. Here, we show that the degree of temporal correlation between continental LIPs and faunal turnover in the Phanerozoic is unlikely to occur by chance, suggesting a causal relationship linking extinctions and continental flood basalts. The relationship is stronger for LIPs with higher estimated eruptive rates and for stage boundaries with higher extinction magnitudes. This suggests LIP magma degassing as a primary kill mechanism for mass extinctions and other intervals of faunal turnover, which may be related to CO_2, SO_2, Cl, and F release. Our results suggest continental LIPs as a major, direct driver of extinctions throughout the Phanerozoic.

volcanology | mass extinctions | carbon cycle | paleontology

Significance

Although the causes of the five largest mass extinctions remain controversial, geochronological improvements have revealed an apparent correlation between large igneous provinces (LIPs) and periods of Phanerozoic faunal turnover. This paper establishes that this relationship is unlikely to occur by chance and defines an eruptive rate threshold, above which known continental LIPs correlate with large extinctions. Continental LIPs also have an approximately linear relationship between their eruptive rate and extinction magnitude. It is difficult to attribute the causality of any one extreme event like an extinction with certainty, but there is an overall correlation between continental LIPs and extinction events that warrants consideration.

Large igneous provinces (LIPs), comprising $>10^5$ km^3 of typically mafic magma with durations generally less than 5 million years, have long been recognized as a distinct category of voluminous volcanic eruptions with the potential to rapidly perturb the environment (1–3). Throughout the Phanerozoic, LIPs have erupted frequently, both on the continents and in the oceans; both U–Pb and Ar–Ar geochronology have been used to date periods of eruptive activity at several such provinces, revealing most of their immense volume to have been emplaced over submillion-year time periods (4).

Fed by extensive dike systems and composed of volatile-bearing volcanics brought up from the deep mantle in plumes, LIPs—especially in their mafic guise as flood basalt provinces—have had pronounced effects on the climate history of Earth (5). Ocean anoxic events (OAEs), global warming (via CO_2 and CH_4), and short-term global cooling (via SO_2) have all been attributed to flood basalt volcanism (3, 6, 7). Most remarkably, at least four of the five mass extinctions of the Phanerozoic coincide with flood basalt eruptions: the Deccan Traps at the Cretaceous–Paleogene (K-Pg) boundary, the Central Atlantic Magmatic Province (CAMP) at the Triassic–Jurassic boundary, the Siberian Traps at the Permo–Triassic boundary, and, more tentatively, the Viluy or Kola-Dnieper Provinces at the Frasnian–Famennian boundary (3, 5, 6); mafic magmatism is speculated at the Late Ordovician mass extinction as well, but has not been correlated with a specific known LIP (3, 8). Other drivers have been proposed for each of these mass extinctions, most notably the Chicxulub impactor at the K-Pg (9), but the temporal coincidence with flood basalts has, nonetheless, attracted significant interest (5) and is difficult to dismiss. Notably, in each such case, the corresponding flood basalt province is continental, not oceanic, despite the fact that many of the largest LIPs (including the two largest known to date) are oceanic (10).

Quantitative Assessment of Temporal Coincidence

While a temporal correlation between flood basalt eruption and biotic extinction has long been qualitatively noted (5), the likelihood of such a correlation arising by chance has not been rigorously quantified across the Phanerozoic. To address this problem, we draw upon three well-established, independent datasets: the Geologic Time Scale (11), the Paleobiology Database (12) [which is the basis for the extinction magnitude calculations of Muscente et al. (13) that are used in this analysis], and the LIP compilation of Ernst (14), updated with the most accurate available geochronology (*Materials and Methods*; *SI Appendix*, Tables S1 and S2).

While the number of Phanerozoic LIPs identified by Ernst (14) far exceeds the number of catastrophic mass extinctions, not every episode of faunal turnover rises to the magnitude of a mass extinction. Indeed, each Phanerozoic stage and period boundary of the Geologic Time Scale is defined on the basis of faunal assemblages, so each of these biological transitions can be taken as a time of potential faunal turnover, much of

Author affiliations: [a]Department of Earth Sciences, Dartmouth College, Hanover, NH 03755; [b]Department of Geosciences, Princeton University, Princeton, NJ 08544; [c]Berkeley Geochronology Center, Berkeley, CA 94709; and [d]Department of Earth and Planetary Science, University of California, Berkeley, CA 94720

Author contributions: T.G. and C.B.K. designed research; T.G. performed research; T.G., P.R.R., and C.B.K. analyzed data; and T.G., P.R.R., and C.B.K. wrote the paper.

The authors declare no competing interest.

This article is a PNAS Direct Submission.

Copyright © 2022 the Author(s). Published by PNAS. This article is distributed under Creative Commons Attribution-NonCommercial-NoDerivatives License 4.0 (CC BY-NC-ND).

[1]To whom correspondence may be addressed. Email: theodore.green@princeton.edu.

This article contains supporting information online at https://www.pnas.org/lookup/suppl/doi:10.1073/pnas.2120441119/-/DCSupplemental.

Published September 12, 2022.

which occurs as a short pulse near the end of the stage (11, 15, 16). We quantify the intensity of this faunal turnover using stage-level genus mean extinction rates calculated by Muscente et al. (13) with data from the Paleobiology Database (12) on August 12, 2018. Although LIPs have been identified throughout Earth history from the Archean to the Phanerozoic (3), the biostratigraphic record underlying our estimates of the timing and severity of faunal turnover is largely restricted to the Phanerozoic, after the advent of skeletal biomineralization. Consequently, our quantitative analysis focuses on the Phanerozoic.

Consider a single geological timescale boundary i occurring at a time constrained by a Riemann-integrable likelihood function $p_i(t)$, reflecting, for example, the Gaussian analytical uncertainty derived from radioisotopic dating of a boundary horizon. For a given time t and time increment δt, the likelihood that boundary i occurs between t and $t + \delta t$ is, by definition,

$$\int_t^{t+\delta t} p_i(t)\,dt = P_i\big|_t^{t+\delta t}, \quad [1]$$

where P_i is the cumulative distribution function corresponding to the likelihood function p_i. We may likewise consider an analogous likelihood function $q_j(t)$ for the eruption of a given increment of magma from LIP j (c.f. *SI Appendix*, Fig. S1). The likelihood of the two events coinciding within a given interval t to $t + \delta t$ if the distributions p and q are independent is then

$$\xi_{ij}\big|_t^{t+\delta t} = P_i\big|_t^{t+\delta t}\; Q_j\big|_t^{t+\delta t}, \quad [2]$$

with a total coincidence likelihood summed over all such intervals within the Phanerozoic (zero through t_{Phan}, with intervals spaced apart by δt), then given by a sum of the form

$$\xi_{ij} = \sum_{n=1}^{t_{Phan}/\delta t} P_i\big|_{t_n}^{t_n+\delta t}\; Q_j\big|_{t_n}^{t_n+\delta t}. \quad [3]$$

Considering that $P_i\big|_t^{t+\delta t}$ is equal to the mean of p over the interval from t to $t + \delta t$ times δt—that is, $\bar{p}_i\big|_t^{t+\delta t}\ \delta t$—we may rewrite Eq. **3** as

$$\xi_{ij} = \sum_{n=1}^{t_{Phan}/\delta t} \bar{p}_i\big|_{t_n}^{t_n+\delta t}\delta t\; \bar{q}_j\big|_{t_n}^{t_n+\delta t}\delta t, \quad [4]$$

which, however, depends on the choice of δt. To remove this dependency, we consider, instead, a scale-invariant version of this coincidence sum

$$\psi_{ij} = \frac{\xi_{ij}}{\delta t} = \sum_{n=1}^{t_{Phan}/\delta t} \bar{p}_i\big|_{t_n}^{t_n+\delta t}\bar{q}_j\big|_{t_n}^{t_n+\delta t}\delta t, \quad [5]$$

which in the limit as δt approaches zero is simply

$$\psi_{ij} = \int_0^{t_{Phan}} p_i(t)\,q_j(t)\,dt, \quad [6]$$

that is, a middle Riemann sum representing the integral of the product of the two likelihood functions p_i and q_j. We define this quantity as the coincidence product ψ_{ij} for boundary i and LIP j. Considering pair-wise all such boundaries i and LIPs j, the total coincidence product for the Phanerozoic (Ψ) is then

$$\Psi = \sum_i \sum_j \psi_{ij}. \quad [7]$$

Using Ψ, then, as our metric, we conduct a simple Monte Carlo simulation, generating $\sim 10^8$ lists of uniformly distributed stage boundaries and calculating the coincidence products for each (*Materials and Methods*). As shown in Fig. 1, we find that the level of correlation between LIPs and periods of faunal turnover far exceeds that expected by chance—occurring in 1 out of every 1.64×10^4 simulations ($P = 6.09 \times 10^{-5}$) when considering the entire list of Phanerozoic stage boundaries and in 1 out of 2.06×10^6 simulations ($P = 4.84 \times 10^{-7}$) when considering only the stage boundaries associated with the five mass extinctions of the Phanerozoic. This relationship is also robust across various subsets of the dataset. The Siberian Traps is the largest LIP associated with a significant extinction, but when it is excluded, the observed correlation between LIPs and stage boundaries still occurs in only 1 out of every 1.60×10^4 simulations ($P = 6.24 \times 10^{-5}$). Even when the five LIPs that are temporally correlated with mass extinctions (the Deccan Traps, CAMP, Siberian Traps, Viluy Province, and Kola-Dnieper Province) are not considered, the observed correlation between LIPs and stage boundary faunal turnover occurs in 1 out of every 9.84×10^3 simulations ($P = 1.02 \times 10^{-4}$). These correlations are still greater than chance and are similar to the P value calculated when the entire LIP list is considered. This demonstrates that the observed correlation between LIPs and Phanerozoic faunal turnover extends to smaller extinction intervals and is not just driven by the mass extinctions. Consistent with previous expectations (5, 17–21), these results provide a first test and confirmation of the statistical significance of the temporal coincidence between LIPs and extinctions.

By contrast, although several Phanerozoic extinctions have been attributed to large bolide impacts (18, 22), we do not find a similarly robust coincidence between Phanerozoic stage boundaries or mass extinction boundaries and the radiometric ages of large impact craters. Fig. 1 shows that much of the correlation observed between impacts and stage-level extinction is driven by the precise coincidence between the Chicxulub impactor and the K-Pg mass extinction, with all P values becoming statistically insignificant when it is not considered. *SI Appendix*, Fig. S2 shows the same effect when impacts are compared only to mass extinction boundaries. While the coincidence products may change with improved geochronology, Fig. 1 demonstrates that LIP eruptions have a correlation with Phanerozoic extinctions that is more robust than the correlation with bolide impacts and extinctions. These results are consistent with a broader trend that becomes clear from a historical examination of the literature; specifically, apart from the K-Pg, proposed impact-extinction correlations have not been confirmed by improved geochronology. For example, while the $\sim$100-km Manicouagan structure (23) was once considered as a potential cause for the end-Triassic mass extinction, it was later found to predate that extinction by about 14 million y (Myr) (24, 25). Where Manicouagan ejecta have been directly located in stratigraphic section, no significant extinction seems to be associated with the event (25, 26). Similarly, the Chesapeake and Popigai impactors—the two largest of the Cenozoic—resolvably predate the Eocene–Oligocene boundary and do not appear to be associated with significant levels of faunal turnover (27–29). Correlation of the Woodleigh impact structure with the Late Devonian mass extinction is likewise doubtful (30). It has been shown previously that smaller impacts, especially those much smaller than Chicxulub, are not associated with significant extinction (22, 31). This analysis supports and extends that conclusion by showing no significant correlation between extinction and impacts smaller than Chicxulub (Fig. 1 and *SI Appendix*, Fig. S2).

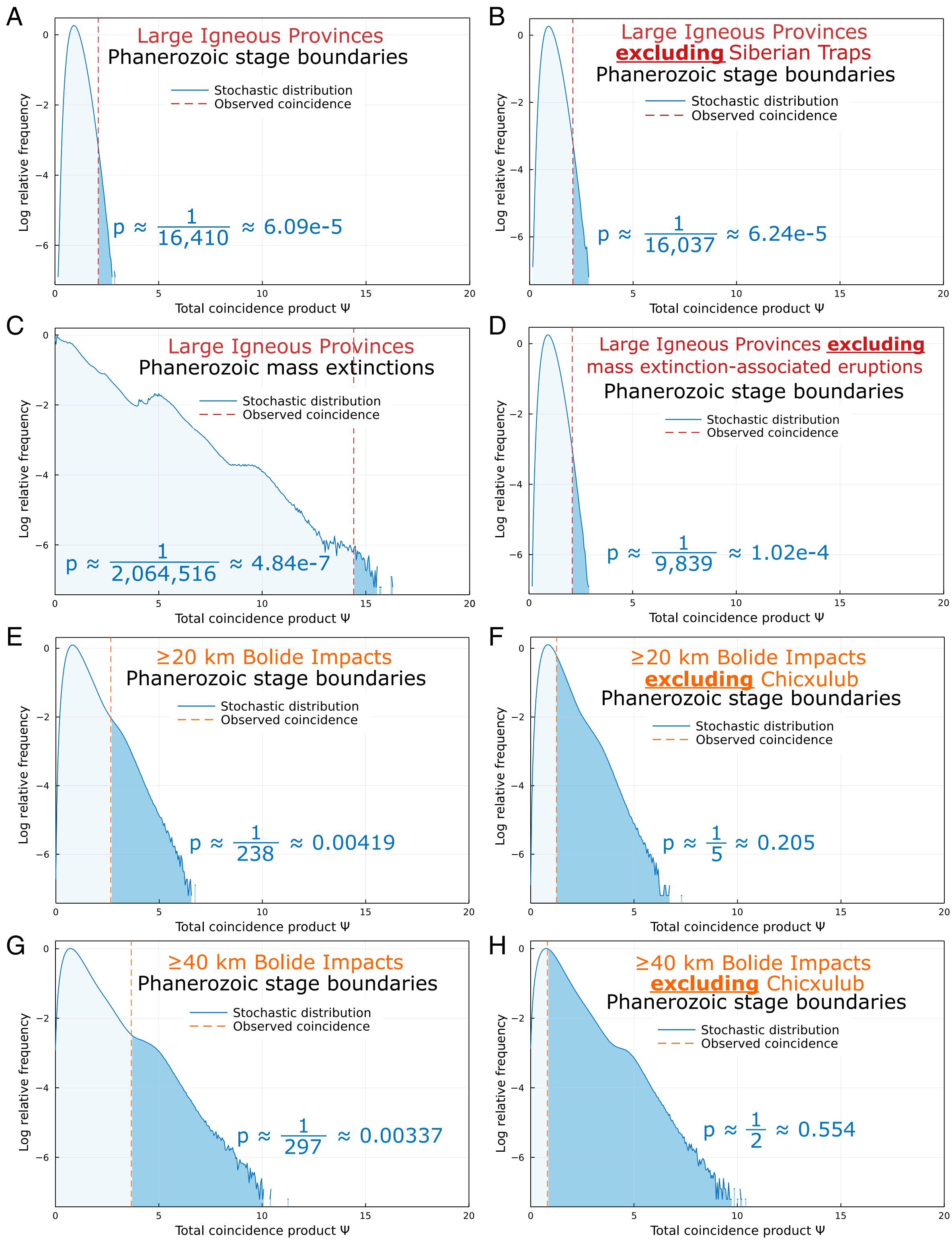

Fig. 1. Relationship between observed and expected coincidence products. The observed coincidence products between all Phanerozoic stage boundaries and all LIPs (*A*), along with the corresponding stochastic distribution (which would result if timescale boundaries were spread randomly throughout the Phanerozoic following a uniform distribution), on a logarithmic *y* scale. The probability that a uniform distribution has a higher coincidence product (Ψ) than observed is given by *P*. Note that the vertical log scale visually distorts the shaded regions compared to the reported *P* values. *B* shows the results for LIPs and stage boundaries when the Siberian Traps, the largest LIP correlated with a severe extinction, is excluded. *C* shows the coincidence products for all LIPs and the five Phanerozoic mass-extinction boundaries. *D* shows the results for LIPs and stage boundaries when all of the LIPs temporally correlated with mass extinctions (the Deccan Traps, CAMP, Siberian Traps, Viluy Province, and Kola-Dnieper Province) are not considered. Even without these large, well-correlated events in *B* and *D*, there is still a statistically significant relationship between LIPs and Phanerozoic extinctions. Below are the observed coincidence products and stochastic distributions of coincidence products for impact events. *E* shows the results for all impacts with diameters ≥20 km and all stage boundaries, while *F* excludes the Chicxulub impactor from consideration. Likewise, *G* shows the results for all impacts with diameters ≥40 km and all stage boundaries, while *H* excludes the Chicxulub. The coincidences between impact events and Phanerozoic extinction are statistically significant only when the Chicxulub impactor is included, indicating that its precise coincidence with the K-Pg mass extinction is primarily responsible for the observed relationship between impacts and extinctions. Since the LIP-extinction coincidence is robust to similar exclusions, this supports a significant temporal relationship between LIPs and faunal turnover over the Phanerozoic.

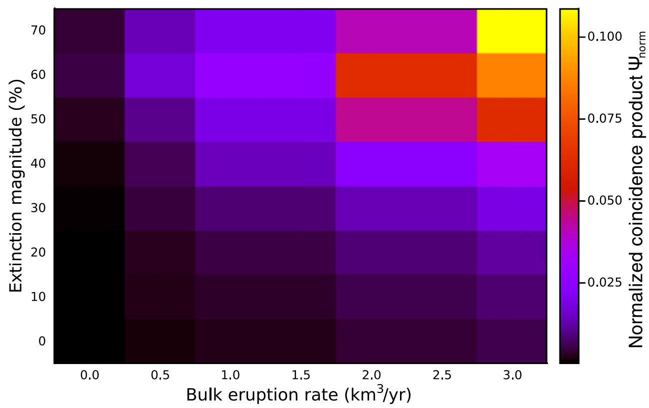

Fig. 2. Greater normalized total coincidence products for larger extinctions and faster bulk eruptive rates. Observed LIP-extinction coincidence products for subsets of the record with varying of extinction severities and eruptive rates, normalized by the maximum possible coincidence product for a subset of that size. The subsets include all LIPs with bulk eruptive rates greater than or equal to the stated bulk eruption rate and all stages with extinction magnitudes greater than or equal to the stated extinction magnitude. For subsets of the record that include only the most severe extinctions and LIPs with the greatest eruptive rates, the observed coincidence products approach the maximum possible values. *SI Appendix*, Fig. S3 shows the same trend when the subsets are nonoverlapping.

If the observed degree of temporal coincidence between LIPs and faunal turnover is the result of a causal relationship, we might further expect larger LIPs to be associated with more severe extinctions. However, such a correlation, at least with absolute LIP magnitude, has not been previously observed (3, 32–34). Rather than absolute magnitude, we consider, instead, "bulk eruption rate"—that is, the total volume of the LIP divided by the best estimate of the total duration over which that bulk was erupted—as a critical parameter. While more difficult to quantify than magnitudes alone (requiring accurate geochronology), rates are highly relevant in the context of critical thresholds in climatic and ecological stability (35–37).

To explore this parameter space, Fig. 2 examines the relative strength of temporal correlation between LIPs and extinctions as a function of both extinction severity and bulk eruption rate. In particular, the maximum possible Ψ diminishes as the number of considered LIPs decreases with an increasingly strict minimum size or rate threshold. This is because the total time span considered remains the same, while the number of events that can potentially be correlated decreases, limiting the observed coincidence product for a given list of events. With that in mind, we consider here as a metric the normalized total coincidence product

$$\Psi_{norm} = \Psi/\Psi_{max}, \quad [8]$$

that is, the Ψ for a given set of LIPs and boundaries divided by the maximum possible Ψ of a set of equivalent size, where each LIP coincides perfectly with an extinction. At higher extinction percents and higher bulk eruptive rates, the normalized total coincidence products increase (Fig. 2). The relatively low value of the highest normalized total coincidence product (0.11; Fig. 2) will likely increase with improved geochronology, but it does indicate that there may be other important factors to consider in the relationship between LIPs and extinctions.

Bulk Eruptive Rate and Extinction Severity

To better understand the potential role of threshold processes in the relationship between bulk eruption rate, LIP duration, and extinction severity, we consider as an analog the framework of Rothman (37), who determined the critical stability threshold of the Phanerozoic biogeochemical carbon cycle in terms of the nondimensionalized mass and nondimensionalized duration of a given carbon-cycle perturbation. While Rothman determined nondimensionalized masses and durations on the basis of carbon isotope excursions, we can easily adapt this framework to our purposes by considering, instead, the equivalently nondimensionalized durations and CO_2 emissions of LIPs, with a degassed CO_2 concentration of 0.5 wt.% (38). This is taken as a reasonable value for CO_2 in basaltic magmas after ref. 38, but a range from 0.2 to 0.5 wt.% is also considered (39) to reflect the potential variation in CO_2 concentrations between different magmatic systems. Most of that CO_2 should be degassed by continental eruptions, but these values may overestimate CO_2 degassing from oceanic LIPs, as more volatiles are trapped in the rocks when they erupt under higher oceanic pressures (40–42). We also adapt this framework to reflect the potentially intermittent nature of volcanic activity by including critical thresholds that represent carbon emissions over 100%, 10%, 1%, and 0.1% of the total event duration (*Materials and Methods*). Hereafter, we consider only nonoceanic LIPs, also known as continental flood basalts (CFBs), because of the potential for decreased volatile degassing in submarine eruptions (40–42) and the lack of preservation of older oceanic LIPs that makes it difficult to extrapolate their effects across the Phanerozoic.

Among all CFBs with quantifiable bulk eruption rates, only the three that coincide with major mass extinction events (the Siberian Traps with the Permo–Triassic, the CAMP with the Triassic–Jurassic, and the Deccan Traps with the K-Pg) plot near the 100% threshold (Fig. 3). These all plot above the 10% critical rate threshold, along with the Emeishan Province that is associated with the severe Capitanian–Wuchiapingian extinction in the late Permian. Other CFBs near, but below, the 10% threshold are generally associated with lesser extinction events or other environmental perturbations like OAEs. For instance, the second phase of the North Atlantic Igneous Province is potentially correlable with the Paleocene–Eocene Thermal Maximum and associated ocean anoxia, while the Parana–Etendeka has been potentially associated with the Valanginian Weissert OAE—yet both lack significant extinctions (5, 13, 43). The lack of extinction associated with these volumetrically significant CFBs has long been a point of discussion (44–46); if the currently available duration (and thus rate) estimates for these CFBs are accurate, this may be simply a consequence of falling below the critical rate threshold, meaning that the rates of CO_2 degassing fall within the range that can be effectively buffered by silicate weathering. However, future geochronological constraints may well result in a reevaluation of these bulk eruption rates. The Karoo–Ferrar LIP, which has been linked to the early Toarcian OAE and a biotic crisis, also falls just below the critical line, but is already well-dated enough that it is unlikely to move above that threshold (47).

The apparent pattern of higher extinction magnitudes for CFBs that plot farther above the 10% critical threshold line in Fig. 3 (i.e., those with greater estimated CO_2 degassing rates) suggests the further possibility of a direct correlation between bulk eruption rate and extinction severity. While CFBs with larger bulk eruptive rates do not necessarily have the largest total volumes in the LIP record, they appear to have much stronger environmental impacts than those that slowly erupt for long periods of time. Indeed, plotting bulk eruption rate vs. extinction magnitude of the largest coincident stage boundary for each of the well-dated ($1\sigma < 0.2\%$) CFBs of the Phanerozoic reveals a clear, positive, approximately linear correlation (Fig. 4)—in sharp contrast to the relative lack of correlation observed when considering total

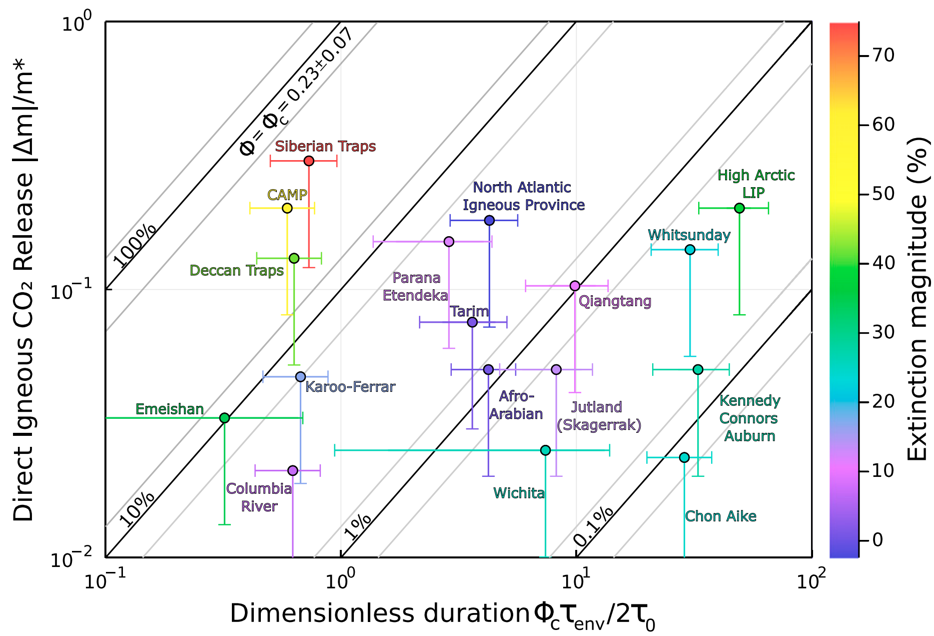

Fig. 3. Carbon-cycle perturbations from continental LIPs relative to the Rothman threshold. The dimensionless carbon-cycle mass perturbation $M = |\Delta m|/m^*$, plotted as a function of the dimensionless timescale of CFB eruption, adapting the nondimensionalizations from Rothman's (37) analysis of C-isotope excursions to flood basalt eruptions. Log scale. The leftmost diagonal (identity) line represents the critical rate threshold $\phi = \phi_c = 0.23 \pm 0.07 = f_{org}$ representing the maximum possible normalized flux perturbation in a mass-conserving carbon cycle with no anomalous sinks or sources (37). The other diagonal lines apply that same critical threshold to events with intermittent CO_2 degassing, occurring over 10%, 1%, or 0.1% of the total duration. CFB provinces that are associated with the highest extinction magnitudes fall closest to the continuous degassing (100%) critical rate threshold and plot above the 10% critical rate threshold. Horizontal error bars reflect 1σ age and ϕ_c uncertainties with the exception of the lower uncertainty on the Emeishan Province, which assumes a minimum τ_{env} of 10,000 y because the small nominal duration of that province causes its start and end age uncertainties to overlap. The 0.5 wt.% CO_2 is taken as a reasonable value after ref. 38, but vertical error bars show the range of potential dimensionless CO_2 masses that result from varying the estimated wt.% CO_2 in the erupted material from 0.2 to 0.5 (39) (*Materials and Methods*).

LIP volume alone (3, 32–34). Moreover, the strength of this correlation appears to suggest that extinction is driven in large part by factors directly proportional to bulk magma eruption or intrusion rate, and not exclusively dependent on, e.g., the type of basin in which a CFB is emplaced or the configuration of the Earth system at the time of the eruption.

While these results suggest a correlation between total magma volume and total volatile emissions at the scale of an entire CFB, such a relationship should not be assumed to hold on smaller spatial scales or timescales. On the contrary, eruption rates per se should not be assumed to act as a proxy for volatile fluxes, especially for volatiles such as CO_2 with high vapor pressures under magmatic conditions. For example, the apparent highest CO_2 flux (and coincident global warming) associated with the Deccan Traps began ~300 kilo annum (ka) prior to the K-Pg extinction and does not coincide with the highest volumetric eruption rate of Deccan lavas (48, 49). This appears to be a case of pre-eruptive (or passive) degassing (50). The decline of this warming began about 150 ka before the extinction and may have been driven by weathering-related drawdown of CO_2 and/or sulfate aerosol emission from Deccan magmas (48). A decoupling of C vs. S degassing is consistent with exsolution of CO_2 preceding that of S, in keeping with the higher solubility of S than of CO_2 in basaltic magmas (41). Indeed, CO_2/SO_2 fractionation as a function of degassing pressure is sufficiently systematic to be used as a measure of magmatic degassing depth (42).

Burgess et al. (51) inferred that, in the case of the Siberian Traps, the main trigger for the Permo–Triassic extinction was CO_2 sourced from supracrustal coal beds that were thermally degassed by interaction with basaltic sills. This represents another version of pre-eruptive degassing, in that erupted magma itself was not the dominant source of CO_2. This differs from the Deccan situation in that there are abundant coal beds known in the substrate of the Siberian Traps, but not in the Deccan. These abundant sedimentary basin-sourced volatiles degassed by the Siberian Traps may explain why the extinction magnitude at the Permo–Triassic boundary is far above the other extinctions, though it is consistent with the trendline that includes CFBs without such nonmagma volatile inputs (Fig. 4). Conversely, the volatile-poor eolian sandstones intruded by the Parana–Etendeka may help explain that eruption's limited environmental impact (44). However, although peaks may be decoupled at finer timescales, high eruption rates must reflect high heat and mass flux on the scale of the lifetime of a CFB. Sedimentary basin-sourced volatiles and pre-eruptive degassing likely play a role in the extinction severity associated with a CFB (32), but does not invalidate the implication that high bulk eruptive rates are mechanistically correlated with significant climate perturbations, leading to major extinctions. Magmatic degassing is the main factor in the critical rate threshold (Fig. 3) and eruptive rate-extinction magnitude linear correlation (Fig. 4) shown here, but passive degassing can explain some of the variability within those relationships.

The critical rate threshold (Fig. 3) and the approximately linear correlation between extinction severity and bulk eruptive rate (Fig. 4) also suggest that any changes in ecosystem stability over time (e.g., refs. 52–54) have not been able to sufficiently buffer the rapid perturbations caused by high-rate CFBs. The lack of severe extinctions associated with more recent eruptive events, such as the North Atlantic Igneous Province, can, given the currently available data, be explained by lower total eruptive rates without invoking a state change in ecosystem stability. Background climate state and boundary conditions, like the $CaCO_3$ saturation state of the oceans (55–57), changes in surface oxygenation (58), and the presence of volatile-rich sediments in the magma ascent path (59),

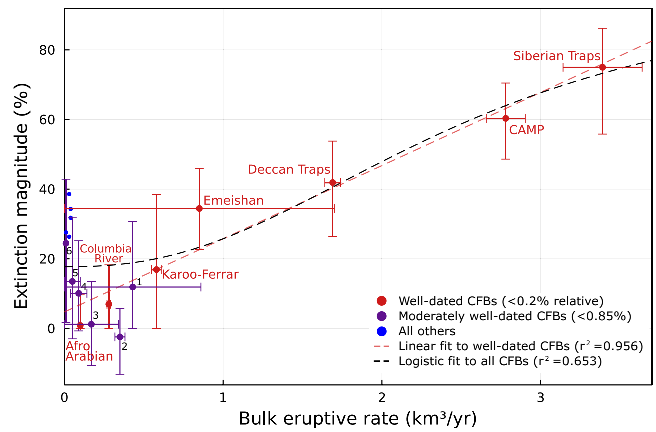

Fig. 4. CFB bulk eruptive rates correlate strongly with extinction severity. Observed correlation between CFBs and extinction magnitudes results in a logistic regression ($r^2 = 0.653$; black) of the form $y = \frac{100-y_0}{1+e^{-k(\ln(x)-x_0)}} + y_0$ with parameters $k = 2.42 \pm 1.24$ (1 SE), $x_0 = 0.92 \pm 0.17$ (1 SE), and $y_0 = 17.71 \pm 3.66$ (1 SE). For the most precisely dated CFBs ($1\sigma < 0.2\%$; red), the observed correlation with extinction magnitude can be approximated by a regression line ($r^2 = 0.956$; red) with a slope of $21.02 \pm 2.02\%/(\mathrm{km}^3/\mathrm{y})$ (1 SE; $t = 10.40$; $P = 0.0001$) and an intercept of $4.73 \pm 3.68\%$ (1 SE; $t = 1.29$; $P = 0.2555$). The intercepts for both regressions are nonzero, potentially because a background extinction rate was not subtracted from the extinction magnitudes from Muscente et al. (13) used here. Moderately well-dated CFBs ($1\sigma < 0.85\%$; purple) broadly fall along the same linear trend: 1, Parana-Etendeka; 2, North Atlantic Igneous Province; 3, Tarim; 4, Qiangtang; 5, Jutland (Skagerrak); and 6, Chon Aike. All other less precisely dated flood basalts are shown in blue. To avoid plotting duplicate correlations for less precisely dated CFBs, boundaries that are correlated with multiple eruptions are shown only with the highest eruptive rate CFB, and CFBs that overlap multiple boundaries are plotted only with the highest extinction magnitude stage. Horizontal error bars reflect 1σ age uncertainties only, not those related to volume. The Emeishan, Parana-Etendeka, and Jutland (Skagerrak) provinces have sufficiently large duration uncertainties to produce negative eruption rates, so those 1σ errors are, instead, set equal to the bulk eruptive rate. Vertical error bars show the range from minimum to maximum extinction magnitude at a given boundary, as calculated by Muscente et al. (13). Exact values are given in *SI Appendix*, Table S5.

may be important for determining climate impacts and play a role in the decreased severity of recent extinctions. However, according to our analyses, these factors are subordinate to eruption rate in determining the severity of extinctions across the Phanerozoic.

Degassing Efficiency and Submarine Flood Basalts

While the results thus far appear to explain most of the Phanerozoic mass extinctions, one major discrepancy remains: In contrast to the CFBs, oceanic LIPs do not appear to obey the same relationship between bulk eruption rate and extinction severity. In particular, the two largest known oceanic flood basalts (the Ontong Java and Kerguelen plateaus), while long in duration, have total volumes well above those of any CFB (10). If oceanic flood basalts fully degassed the same concentration of CO_2 as their continental counterparts, these LIPs would fall well above the 10% critical rate threshold (*SI Appendix*, Fig. S4), yet are associated with lower extinction magnitudes than CFB eruptions above that threshold. The Ontong Java Province even falls above the 100% critical threshold.

One possible solution may involve decreased magma degassing in submarine eruptions due to the confining pressure of the overlying water column. Firstly, for volatiles with low vapor pressures (including SO_2, Cl, and F), exsolution is a strong function of pressure (41, 42). Gaillard et al. (40), for example, estimate six times less SO_2 exsolution for magmas erupted under 1 km of water than at the surface on the basis of the increased solubility of such volatiles in basaltic magmas at increased pressure. Secondly, even once exsolved, volatiles may be physically trapped in vesicles or other pore spaces. Such physical trapping would affect all volcanic volatiles, including CO_2, and is dramatically enhanced in submarine magmas to the extent that some seafloor basalts spontaneously and violently fracture upon being raised to the surface due to the expansion of the compressed CO_2 and other volatiles trapped in their vesicles (60).

In this context, it is perhaps notable that for the only attested historical analog of a CFB eruption, the $\sim$12-km^3 1783 to 1784 Laki fissure eruption in Iceland, records suggest marked direct mortality of humans (with an estimated total of some $\sim$50,000 across Europe), livestock, and both inland and coastal fish populations—all mediated by SO_2, Cl, and F, not CO_2 (61–63). The ecological effects of these volatiles during the Laki eruption may not directly parallel those expected to produce the genus-level marine extinctions analyzed here. Still, it is a notable, if small-scale, example of how such basaltic eruptions can negatively impact the biosphere, including coastal marine populations. The most significant climatic consequence of these eruptions, an estimated $\sim$1 °C decrease in Northern Hemisphere surface temperatures for 2 to 3 y following the eruption, is likewise a result of stratospheric sulfate aerosols (62) and independent of CO_2. Nonetheless, we also observe that the CO_2-based critical rate threshold (Fig. 3) does effectively separate CFBs associated with mass extinctions from those with more limited environmental impacts—perhaps an unlikely coincidence if CO_2 itself played no significant role in extinction severity. In this context, the potential temporal decoupling of volcanic $CO2_2$ and SO_2 emissions by pre-eruptive degassing may be especially significant. Given the greater volatility and expected earlier (and deeper-sourced) pre-eruptive degassing of CO_2, we may expect a general pattern that features early pre-eruptive (CO_2-driven) warming to precede rapid syn-eruptive (SO_2-driven) cooling, followed by a return to warming as the emission of SO_2 aerosols declines. Such climate whiplash may be expected to accentuate biotic stress, where the ecosystem must adapt to rapidly reversing warming and cooling trends, along with both CO_2- and SO_2-driven acidification (64).

CFBs Drive Phanerozoic Extinctions

Our results suggest that CFB eruptions are a primary known driver of mass extinction throughout the Phanerozoic. While it is difficult to assign the causal mechanism for any single given extinction on the basis of temporal correlation alone, the broader correlation across the Phanerozoic between faunal turnover and LIP eruptions (Fig. 1) is extraordinarily unlikely to have arisen by chance. In the absence of an external mechanism producing the mantle plumes that drive LIP eruptions and the environmental perturbations that lead to extinctions, this degree of correlation suggests a causal relationship. This observed correlation between extinction and LIP eruption pertains both for mass extinctions and lesser faunal turnovers, but is strongest for boundaries with higher rates of extinction and flood basalts with higher bulk eruptive rates (Fig. 2).

The additional correlation we observe between bulk eruption rate and extinction magnitude (Fig. 4) allows a direct estimation of the degree to which the severity of a given mass extinction corresponds with the expected severity if the extinction were caused by a coincident CFB eruption alone. The linearity of this correlation indicates that the deadly consequences of CFBs are, in general, directly proportional to their total volumetric eruption rate, though intrusive and passive degassing may well play a critical role in the timing of volatile release. Additionally, given the generally gradual nature of flood basalt volatile release on biological timescales, our results reinforce the expectation (35–37) that threshold processes—be they ecological, biogeochemical, or climatic—play a major role in mass extinction. Continued improvements in the high-precision geochronology of flood basalts and continued biostratigraphic study of faunal turnover and extinction in expanded sedimentary sections throughout the Phanerozoic will continue to refine our understanding of these correlations and of the exact mechanisms implicated therein.

Although a correlation between LIPs and mass extinctions is now well established, there is still much resistance to the notion that the Deccan Traps played any significant role in driving species extinction at the K-Pg boundary (65, 66). In this context, it has not escaped our notice that the correlation observed in Fig. 4 between CFB eruptive rates and extinction magnitude implies that the Deccan Traps may have produced a sizeable extinction around the K-Pg boundary, even without the coincidence of the Chicxulub impactor. It has long been noted that the Chicxulub impactor is precisely coincident with and expected to drive extremely rapid extinction at the K-Pg boundary (65, 67, 68), but high-latitude records are compatible with gradual extinction leading up to the boundary, which may be attributable to the longer-term environmental stresses of the Deccan Traps eruptions (69–71). The position of the K-Pg extinction above the regression line in Fig. 4 is consistent with the hypothesis that the Chicxulub impactor increased the severity and brevity of the K-Pg extinction, but the role of the Deccan Traps as a preimpact stressor and extinction mechanism should not be minimized. Following the linear extrapolation in Fig. 4, the 41.9% extinction observed at the K-Pg boundary is within the uncertainty of the $40.3 \pm 5.1\%$ (1σ) extinction predicted by the eruption rate of the Deccan Traps. Moreover, despite the emphasis frequently placed on bolide impact as a driver of the most charismatic extinction of the Phanerozoic, a significant coincidence between impacts and mass extinctions is not borne out beyond the K-Pg.

Further exploration of this correlation between CFBs and extinctions, along with detailed geographical constraints on faunal abundance data, could potentially illustrate a "common cause" for the observed association between faunal turnover and relative sea-level fall (72). The mantle plumes that drive CFB volcanism are known to cause domal uplift of the crust with an amplitude on the order of 1,000 m and wavelength on the order of 1,000 km, persisting for up to several Myr (73). With relative continental uplift (and, thus, relative sea-level fall) from this mantle upwelling and associated thermal anomalies, we may expect CFBs, but not their oceanic equivalents, to be directly correlated with the regression and disconformity often seen during the intervals of faunal turnover. This regression and loss of habitat in the epicratonic marine realm may then compound the direct stresses imposed by volcanic volatile emissions that this work suggests are a primary kill mechanism during Phanerozoic extinction intervals.

Materials and Methods

We used the extinction record calculated by Muscente et al. (13) from Paleobiology Database records (12) to evaluate the faunal turnover at each geologic stage boundary (*SI Appendix*, Table S1). The Geologic Time Scale 2012 (11) was used to define the date and uncertainty of each of these stages. The LIP compilation of Ernst (14) was updated with the most precise available geochronology (*SI Appendix*, Table S2) and compared with the Muscente et al. calculations (13) (*SI Appendix*, Table S1) to analyze the coincidence between LIPs and periods of faunal turnover.

For each LIP, we define an estimated eruptive duration that includes a majority of the known eruptive products, using the most disparate high-precision-and-accuracy age bounds to define the start and end ages (*SI Appendix*, Table S2). The eruptive rate for each Phanerozoic LIP was then calculated by dividing the best estimate of the total LIP volume by the eruptive duration to get an average rate in terms of km^3/y over the bulk of the eruptive period (*SI Appendix*, Table S2). LIPs erupted before the Carboniferous are more heavily eroded and do not have robust volume estimates, so their eruptive rates were not calculated.

While the likelihood functions of geological timescale boundaries are generally Gaussian, the separate Gaussian distributions for LIP start and end ages require that the likelihood functions for LIPs be defined in terms of the product of those two normal cumulative distribution functions: one representing the likelihood that LIP eruption has begun and a second representing the likelihood that LIP eruption has ceased (c.f. *SI Appendix*, Fig. S1). Consequently, the integral of the product of p_i and q_j given in Eq. **6** generally cannot be solved analytically. Instead, we integrate this equation numerically over a time interval from 10 SDs before the mean start age to 10 SDs after the mean end age for each LIP.

By generating some 10^n uniform random lists of timescale boundaries (i.e., synthetic boundary lists, where each timescale boundary is distributed as $Unif(0, t_{Phan})$, with t_{Phan} as the start time of the Phanerozoic) for some sufficiently large n, it is possible to determine numerically what proportion, if any, result in a higher coincidence product than the real list of geologic timescale boundaries and Phanerozoic LIPs (Fig. 1 and *SI Appendix*, Table S1). When a one-sample exact Kolmogorov–Smirnov test was applied to the observed distribution of Phanerozoic stage boundaries before the Quaternary (*SI Appendix*, Fig. S5), the 95% confidence outcome could not reject the null hypothesis that the Phanerozoic stage boundaries are drawn from a uniform distribution (two-sided $P = 0.8141$). This supports the use of these uniform random boundary lists for calculating coincidence products. The probability (P) is given by dividing the number of random lists that have a coincidence product larger than that of the real list of timescale boundaries by the number of uniform random lists generated.

To efficiently generate this large number of uniform random boundary lists and calculate their coincidence products, we wrote a scalable Julia program (74) (available at https://github.com/Theodore-Green/LIP-Extinction-Correlations) (75) using MPI.jl for distributed-memory parallel programming by message passing (76) and VectorizedRNG.jl for random number generation using a vectorized Xoshiro256++ (77) algorithm. We then ran this program on the Dartmouth College linux cluster *Discovery*, completing 10^8 simulations for each of the LIP log relative frequency plots in Fig. 1.

A similar approach was used to generate the log relative frequency plots for impacts in Fig. 1. The impact compilation of Schmieder and Kring (23) was combined with estimated impact crater diameters from the Earth Impact Database (78) (*SI Appendix*, Table S3) and, like the LIP record, compared with the stage boundary extinction record (*SI Appendix*, Table S1) to analyze the coincidence between Phanerozoic impacts and periods of faunal turnover. Since the bolide impacts have only one Gaussian event age instead of the separate start and end ages of LIPs, the integral of the product of p_i and q_j given in Eq. **6** generally can be solved analytically for impact events. Synthetic boundary lists were generated and coincidence products calculated in the same manner as previously described for LIPs. The observed coincidences for impact crater diameters $\geq$20 km and $\geq$40 km with stage-level and mass extinctions are statistically significant (Fig. 1 and *SI Appendix*, Fig. S2). However, the Chicxulub impactor is obviously coincident with the K-Pg mass extinction, based on the way that boundary is defined (11), so its role in producing the correlations seen in Fig. 1 and *SI Appendix*, Fig. S2 is explored by excluding it from the analyses in those figures as well. The values for P (the probability that a uniform distribution has a higher coincidence product [Ψ] than observed) indicate that the observed correlation between impacts and faunal turnover likely could be produced by chance without the Chicxulub impactor, indicating that the observed trends are driven primarily by that one event. This shows that other Phanerozoic impactors, all smaller than the Chicxulub, do not show the proposed correlation with extinctions (18, 22).

To test whether the observed LIP-extinction coincidences were likewise being driven by a single event, we repeated the experiments for Fig. 1 after removing the Siberian Traps from the list of considered LIPs. Even without this LIP precisely correlated with the Permo–Triassic mass extinction (51), Fig. 1 and *SI Appendix*, Fig. S6 show a relationship between LIPs and extinction that is unlikely to be produced by chance. Similarly, this was repeated for LIPs and stage boundaries when all of the LIPs temporally correlated with mass extinctions (the Deccan Traps, CAMP, Siberian Traps, Viluy Province, and Kola-Dnieper Province) were not considered. The relationship between LIPs and Phanerozoic extinctions remains statistically significant, even without these large, well-correlated events (Fig. 1). This demonstrates that the correlation between LIPS and Phanerozoic extinctions is robust and applicable even to smaller LIPs.

We also repeated the analyses just for CFBs. CFBs, like the whole LIP list, show observed coincidence products that are unlikely to be produced by chance, even when the eruptions most precisely correlated with extinctions are not considered (*SI Appendix*, Fig. S7). This provides confidence that the analyses shown in Figs. 3 and 4, which only consider CFBs, reflect the same trend observed in Fig. 1 with all LIPs.

The trend in Fig. 2 was also tested to see if it was driven primarily by the largest events. *SI Appendix*, Fig. S3 shows the results from dividing the considered LIP list into nonoverlapping categories of low, low-medium, medium-high, and high eruptive rates and extinction magnitudes. Even without allowing events to appear in multiple categories like Fig. 2, the trend of the observed coincidence product approaching the maximum possible coincidence product for a given list (normalized total coincidence product increasing) at higher eruptive rates and extinction magnitudes holds (*SI Appendix*, Fig. S3).

Particularly at these high eruptive rates that have stronger correlations with extinction events, CO_2 degassing from flood basalt magmas would be a significant perturbation to the Earth system that, like the carbon isotope excursions explored by Rothman (37, 79), should result in mass extinction when the rate of environmental change exceeds a critical threshold. Following Rothman (37), the dimensionless inorganic carbon mass perturbation is

$$M = \frac{|\Delta m|}{m^*}, \qquad \textbf{[9]}$$

where $m^* = 139,200$ Pg is the steady-state value of inorganic CO_2 in the oceans [from the 38,000-Pg preindustrial reservoir of inorganic C (80) used in Rothman's calculations] and Δm is the mass change. The dimensionless duration is

$$T = \frac{\phi_c * \tau_{env}}{2\tau_0}, \qquad \textbf{[10]}$$

where ϕ_c is equal to the organic burial fraction through geologic time of 0.23 ± 0.07 and the dimensionless, maximum, normalized flux (ϕ) for each event (37). τ_{env} is the duration of the event, and τ_0 is the 140,000-y turnover time for inorganic carbon in the oceans (37). Plotting the dimensionless duration of an event against its corresponding dimensionless carbon mass change shows where each event lies in relation to the critical threshold, defined by Rothman (37) as the identity line where

$$\phi = \phi_c = 0.23 \pm 0.07. \qquad \textbf{[11]}$$

Those events that lie above the critical threshold are expected to result in mass extinctions and other environmental catastrophes. Rather than investigate carbon isotope events, we adapt this framework to LIP eruptions and associated carbon fluxes. The dimensionless mass is found by using a value of 0.5 wt.% degassed CO_2 for basaltic magmas (38). This is taken as a reasonable, but potentially high, value (38), so a range from 0.2 to 0.5 wt.% CO_2 is used for error bars on that value (39). That value for pre-eruptive CO_2 content is then used in order to calculate the direct CO_2 release from a given LIP eruption as the Δm value in the dimensionless mass term. The same wt.% CO_2 is used for oceanic and continental LIPs here, but higher ocean pressures may have decreased the amount of that CO_2 released by trapping gas in bubbles within the magma (i.e., popping rocks) (60, 81). The duration of a given LIP (*SI Appendix*, Table S2) is used for τ_{env} in calculating the dimensionless duration of the event. To account for LIP eruptions that may occur in distinct pulses, rather than assuming constant output over the entire duration, we also define critical thresholds for events that input C in pulses comprising 10%, 1%, and 0.1% of their total durations. Fig. 3 shows the dimensionless duration and dimensionless C mass perturbation for CFBs, while *SI Appendix*, Fig. S4 shows the results for oceanic and continental LIPs. The LIP points are colored according to the extinction magnitude at the timescale boundary that coincides with that eruption.

SI Appendix, Fig. S8 applies the same framework to the present oceanic uptake of CO_2 and that predicted by 2100 based on the various emissions scenarios (Shared Socio-economic Pathway [SSP] 1.9, 2.6, 4.5, 7.0, and 8.5) defined in the 2021 Intergovernmental Panel on Climate Change report (82). These modern inputs are plotted on the same axes as the CFBs shown in Fig. 3, but the short duration necessitates an adaption of the critical threshold. For events with durations less than 10,000 y, the critical size

$$M_c = 0.0082 \pm 0.0041, \qquad \textbf{[12]}$$

is used to define the critical threshold instead of the rate equation in order to account for the minimum amount of time necessary for the ocean carbon cycle to respond to an influx of material (37). The present oceanic CO_2 uptake and that for the low-emission SSP 1.9 scenario fall below the critical size threshold, but the other emission scenarios plot at or above the critical threshold for modern carbon-cycle inputs. This indicates that CO_2 inputs since 1850 are comparable to the CFBs that are associated with the highest extinction magnitudes.

For Fig. 4, the ratio of the average LIP start and end times and the uncertainties on those ages is used to define the relative uncertainty (1σ error) of each eruption. The most precisely dated CFBs have relative uncertainties of less than 0.2% and are included in the linear correlation. Moderately well-dated CFBs are those with 1σ error less than 0.85%. Moderately well-dated CFBs are not included in the linear correlation, but tend to fall near the line. With improved dating, these eruptions may shift closer to the line. The proposed eruptive durations of many less-precisely dated CFBs ($1\sigma > 0.2\%$) overlap multiple geologic timescale boundaries. For these, the CFB with the highest eruptive rate at a given boundary is considered, and, when a CFB overlaps more than one boundary, only the boundary with the highest extinction magnitude is plotted in Fig. 4. All the CFBs are included in the logistic regression, which constrains the function to the physically possible range of values of the data (0 to 100%). The logistic trend is approximately linear in the considered range. Best estimates of volume are used throughout, but volume remains difficult to constrain for many LIPs. For well-dated and moderately well-dated CFBs, the extinction magnitudes predicted from the linear trend are listed and compared to the extinction magnitude at the corresponding boundary in *SI Appendix*, Table S5.

The precisely dated CFBs are split into two categories (bulk eruptive rates <1 km^3/y and ≥ 1 km^3/y) to plot the two regression lines shown in *SI Appendix*, Fig. S9. Both categories show a positive, linear relationship between bulk eruptive rate and extinction magnitude, though they have different slopes and intercepts. The regression line for the higher rate eruptions more closely matches the overall trend, which suggests that those high-rate CFBs are a strong influence on the observed trend, but the linear trend in each category is still interesting in comparison to the lack of observed correlation between volume and extinction severity (3, 32–34).

Data, Materials, and Software Availability. All datasets used are included as *SI Appendix*, Tables S1–S3. The code, datasets, and coincidence product results for this project are available at GitHub (https://github.com/Theodore-Green/LIP-Extinction-Correlations) (75). Previously published data were used for this work (11, 13, 14, 23, 78).

ACKNOWLEDGMENTS. We thank A. Gelb, E. Geyman, W. Leavitt, Y. Lee, E. Osterberg, G. Pease, B. Schoene, S. Slotznick, and M. Stroud for valuable discussion. T.G. was supported by a Dartmouth College Senior Fellowship. P.R.R. was supported by the Ann and Gordon Getty Foundation and NSF Grants EAR-1615021 and EAR-1736737.

1. M. Coffin, O. Eldholm, eds., "Large igneous provinces" (Joint Oceanographic Institutions/US Scientific Advisory Committee Workshop Report, Cannon Technical Report, The University of Texas at Austin Institute for Geophysics, Austin, TX, 1991).
2. M. Coffin, O. Eldholm, Volcanism and continental break-up: A global compilation of large igneous provinces (Special Publications, Geological Society, London, 1992), vol. 68, pp. 17–30.
3. R. E. Ernst, N. Youbi, How Large Igneous Provinces affect global climate, sometimes cause mass extinctions, and represent natural markers in the geological record. *Palaeogeogr. Palaeoclimatol. Palaeoecol.* **478**, 30–52 (2017).
4. R. E. Ernst, W. Bleeker, U. Soderlund, A. C. Kerr, Large Igneous Provinces and supercontinents: Toward completing the plate tectonic revolution. *Lithos* **174**, 1–14 (2013).
5. V. E. Courtillot, P. R. Renne, On the ages of flood basalt events. *C. R. Geosci.* **355**, 113–140 (2003).

6. J. Kasbohm, B. Schoene, S. Burgess, "Radiometric constraints on the timing, tempo, and effects of large igneous province emplacement" in *Large Igneous Provinces: A Driver of Global Environmental and Biotic Changes*, R. E. Ernst, A. J. Dickson, A. Bekker, Eds. (John Wiley and Sons, Inc., Hoboken, NJ, ed. 1, 2021), pp. 27–68.
7. L. M. E. Percival *et al.*, Globally enhanced mercury deposition during the end-Pliensbachian extinction and Toarcian OAE: A link to the Karoo–Ferrar Large Igneous Province. *Earth Planet. Sci. Lett.* **428**, 267–280 (2015).
8. D. S. Jones, A. M. Martini, D. A. Fike, K. Kaiho, A volcanic trigger for the Late Ordovician mass extinction? Mercury data from south China and Laurentia. *Geology* **45**, G38940.1 (2017).
9. W. Alvarez *et al.*, Impact theory of mass extinctions and the invertebrate fossil record. *Science* **223**, 1135–1141 (1984).
10. N. I. Deligne, H. Sigurdsson, "Global rates of volcanism and volcanic episodes" in *The Encyclopedia of Volcanoes*, H. Sigurdsson, B. Houghton, S. McNutt, H. Rymer, J. Stix, Eds. (Academic Press, Amsterdam, 2015), pp. 265–272.
11. F. M. Gradstein, J. G. Ogg, M. D. Schmitz, G. M. Ogg, *The Geologic Time Scale 2012* (Elsevier, Amsterdam, 2012).
12. PBDB, The Paleobiology Database. https://paleobiodb.org/#/. Accessed 23 March 2022.
13. A. Muscente *et al.*, Appearance and disappearance rates of Phanerozoic marine animal paleocommunities. *Geology* **50**, 341–345 (2021).
14. R. E. Ernst, *Large Igneous Provinces* (Cambridge University Press, Cambridge, UK, 2014).
15. S. E. Peters, N. A. Heim, Macrostratigraphy and macroevolution in marine environments: Testing the common-cause hypothesis. *Geol. Soc. Lond. Spec. Publ.* **358**, 95–104 (2011).
16. M. Foote, Pulsed origination and extinction in the marine realm. *Paleobiology* **31**, 6–20 (2005).
17. R. V. White, A. D. Saunders, Volcanism, impact and mass extinctions: Incredible or credible coincidences? *Lithos* **79**, 299–316 (2005).
18. M. R. Rampino, K. Caldeira, Comparison of the ages of large-body impacts, flood-basalt eruptions, ocean-anoxic events and extinctions over the last 260 million years: A statistical study. *Int. J. Earth Sci.* **107**, 601–606 (2018).
19. N. C. Arens, I. D. West, Press-pulse: A general theory of mass extinction? *Paleobiology* **34**, 456–471 (2008).
20. P. R. Vogt, Evidence for global synchronism in mantle plume convection, and possible significance for geology. *Nature* **240**, 338–342 (1972).
21. M. R. Rampino, R. B. Stothers, Flood basalt volcanism during the past 250 million years. *Science* **241**, 663–668 (1988).
22. M. R. Rampino, Relationship between impact-crater size and severity of related extinction episodes. *Earth Sci. Rev.* **201**, 102990 (2020).
23. M. Schmieder, D. A. Kring, Earth's impact events through geologic time: A list of recommended ages for terrestrial impact structures and deposits. *Astrobiology* **20**, 91–141 (2020).
24. J. P. Hodych, G. R. Dunning, Did the Manicouagan impact trigger end-of-Triassic mass extinction? *Geology* **20**, 51–54 (1992).
25. M. Clutson, D. Brown, L. Tanner, "Distal processes and effects of multiple Late Triassic terrestrial bolide impacts: Insights from the Norian Manicouagan Event" in *The Late Triassic World*, L. Tanner, Ed. (Topics in Geobiology, Springer, Cham, Switzerland, 2018), vol. 46, pp. 127–187.
26. T. Onoue *et al.*, Deep-sea record of impact apparently unrelated to mass extinction in the Late Triassic. *Proc. Natl. Acad. Sci. U.S.A.* **109**, 19134–19139 (2012).
27. R. Bottomley, R. Grieve, D. York, V. Masaitis, The age of the Popigai impact event and its relation to events at the Eocene/Oligocene boundary. *Nature* **388**, 365–368 (1997).
28. V. A. Fernandes *et al.*, 40Ar-39Ar step heating ages of North American tektites and of impact melt rock samples from the Chesapeake Bay impact structure. *Geochim. Cosmochim. Acta* **255**, 289–308 (2019).
29. G. J. Retallack *et al.*, Eocene-Oligocene extinction and paleoclimatic change near Eugene, Oregon. *Geology* **116**, 817–839 (2004).
30. P. R. Renne, W. Reimold, C. Koeberl, R. Hough, P. Claeys, Comment on: "K–Ar evidence from illitic clays of a Late Devonian age for the 120 km diameter Woodleigh impact structure, Southern Carnarvon Basin, Western Australia", by I.T. Uysal, S.D. Golding, A.Y. Glikson, A.J. Mory and M. Glikson [Earth Planet. Sci. Lett. 192 (2001) 218–289]. *Earth Planet. Sci. Lett.* **201**, 247–252 (2002).
31. D. M. Raup, "Impact as a general cause of extinction: A feasibility test" in *Global Catastrophes in Earth History: An Interdisciplinary Conference on Impacts, Volcanism, and Mass Mortality* (GSA Special Papers, Geological Society of America, Boulder, CO, 1988), vol. 673, pp. 148–149.
32. C. Ganino, N. T. Arndt, Climate changes caused by degassing of sediments during the emplacement of large igneous provinces. *Geology* **37**, 323–326 (2009).
33. D. P. Bond, P. B. Wignall, "Large igneous provinces and mass extinctions: An update" in *Volcanism, Impacts, and Mass Extinctions: Causes and Effects*, G. Keller, A. C. Kerr, Eds. (Geological Society of America, Boulder, CO, 2014).
34. M. E. Clapham, P. R. Renne, Flood basalts and mass extinctions. *Annu. Rev. Earth Planet. Sci.* **47**, 275–303 (2019).
35. T. Säterberg, S. Sellman, B. Ebenman, High frequency of functional extinctions in ecological networks. *Nature* **499**, 468–470 (2013).
36. K. Siteur, M. B. Eppinga, A. Doelman, E. Siero, M. Rietkerk, Ecosystems off track: Rate-induced critical transitions in ecological models. *Oikos* **125**, 1689–1699 (2016).
37. D. H. Rothman, Thresholds of catastrophe in the Earth system. *Sci. Adv.* **3**, e1700906 (2017).
38. S. Self, T. Thordarson, M. Widdowson, Gas fluxes from flood basalt eruptions. *Elements* **1**, 283–287 (2005).
39. P. J. Wallace, T. Plank, M. Edmonds, E. H. Hauri, "Volatiles in magmas" in *The Encyclopedia of Volcanoes*, H. Sigurdsson, Ed. (Academic Press, Amsterdam, ed. 2, 2015), pp. 163–183.
40. F. Gaillard, B. Scaillet, N. T. Arndt, Atmospheric oxygenation caused by a change in volcanic degassing pressure. *Nature* **478**, 229–232 (2011).
41. M. Edmonds, New geochemical insights into volcanic degassing. *Philos. Trans. R. Soc., Math. Phys. Eng. Sci.* **366**, 4559–4579 (2008).
42. H. Shinohara, A. Aiuppa, G. Giudice, S. Gurrieri, M. Liuzzo, Variation of H_2O/CO_2 and CO_2/SO_2 ratios of volcanic gases discharged by continuous degassing of Mount Etna volcano, Italy. *J. Geophys. Res.* **113**, 1556 (2008).
43. A. D. Saunders, Two LIPs and two earth-system crises: The impact of the North Atlantic igneous province and the Siberian Traps on the earth-surface carbon cycle. *Geol. Mag.* **153**, 201–222 (2016).
44. P. R. Renne *et al.*, The age of Parana flood volcanism, rifting of Gondwanaland, and the Jurassic-Cretaceous boundary. *Science* **258**, 975–979 (1992).
45. P. Wignall, The link between large igneous province eruptions and mass extinctions. *Elements* **1**, 293–297 (2005).
46. S. C. Dodd, C. Mac Niocaill, A. R. Muxworthy, Long duration ($>$4 Ma) and steady-state volcanic activity in the early Cretaceous Paraná–Etendeka Large Igneous Province: New palaeomagnetic data from Namibia. *Earth Planet. Sci. Lett.* **414**, 16–29 (2015).
47. S. D. Burgess, S. A. Bowring, T. H. Fleming, D. H. Elliot, High-precision geochronology links the Ferrar large igneous province with early-Jurassic ocean anoxia and biotic crisis. *Earth Planet. Sci. Lett.* **415**, 90–99 (2015).
48. C. J. Sprain *et al.*, The eruptive tempo of Deccan volcanism in relation to the Cretaceous-Paleogene boundary. *Science* **363**, 866–870 (2019).
49. B. Schoene *et al.*, U-Pb constraints on pulsed eruption of the Deccan Traps across the end-Cretaceous mass extinction. *Science* **363**, 862–866 (2019).
50. A. H. Nava *et al.*, Reconciling early Deccan Traps CO_2 outgassing and pre-KPB global climate. *Proc. Natl. Acad. Sci. U.S.A.* **118**, e2007797118 (2021).
51. S. D. Burgess, J. D. Muirhead, S. A. Bowring, Initial pulse of Siberian Traps sills as the trigger of the end-Permian mass extinction. *Nat. Commun.* **8**, 164 (2017).
52. H. Weissert, Mesozoic C-cycle perturbations and climate: Evidence for increased resilience of the Cretaceous biosphere to greenhouse pulses. *Can. J. Earth Sci.* **56**, 1366–1374 (2019).
53. J. L. Payne, A. Bachan, N. A. Heim, P. M. Hull, M. L. Knope, The evolution of complex life and the stabilization of the Earth system. *Interface Focus* **10**, 20190106 (2020).
54. P. B. Wignall, "Pangea's death and the rise of resilience" in *The Worst of Times: How Life on Earth Survived Eighty Million Years of Extinctions* (Princeton University Press, Princeton, NJ, 2015), pp. 154–176.
55. RE Zeebe, P Westbroek, A simple model for the $CaCO_3$ saturation state of the ocean: The "Strangelove," the "Neritan," and the "Cretan" Ocean. *Geochem. Geophys. Geosyst.* **4**, 1104 (2003).
56. A. Ridgwell, A Mid Mesozoic Revolution in the regulation of ocean chemistry. *Mar. Geol.* **217**, 339–357 (2005).
57. J. L. Payne, L. R. Kump, Evidence for recurrent Early Triassic massive volcanism from quantitative interpretation of carbon isotope fluctuations. *Earth Planet. Sci. Lett.* **256**, 264–277 (2007).
58. R. G. Stockey, A. Pohl, A. Ridgwell, S. Finnegan, E. A. Sperling, Decreasing Phanerozoic extinction intensity as a consequence of Earth surface oxygenation and metazoan ecophysiology. *Proc. Natl. Acad. Sci. U.S.A.* **118**, e2101900118 (2021).
59. H. Svensen *et al.*, Release of methane from a volcanic basin as a mechanism for initial Eocene global warming. *Nature* **429**, 542–545 (2004).
60. P. Sarda, D. Graham, Mid-ocean ridge popping rocks: Implications for degassing at ridge crests. *Earth Planet. Sci. Lett.* **97**, 268–289 (1990).
61. T. Thordarson, S. Self, N. Oskarsson, T. Hulsebosch, Sulfur, chlorine, and fluorine degassing and atmospheric loading by the 1783-1784 AD Laki (Skaftár Fires) eruption in Iceland. *Bull. Volcanol.* **58**, 205–225 (1996).
62. A. L. Chenet, F. Fluteau, V. Courtillot, Modelling massive sulphate aerosol pollution, following the large 1783 Laki basaltic eruption. *Earth Planet. Sci. Lett.* **236**, 721–731 (2005).
63. C. Oppenheimer, *Eruptions that Shook the World* (Cambridge University Press, Cambridge, UK, 2011).
64. L. Li, G. Keller, Abrupt deep-sea warming at the end of the Cretaceous. *Geology* **26**, 995–998 (1998).
65. P. M. Hull *et al.*, On impact and volcanism across the Cretaceous-Paleogene boundary. *Science* **367**, 266–272 (2020).
66. A. A. Chiarenza *et al.*, Asteroid impact, not volcanism, caused the end-Cretaceous dinosaur extinction. *Proc. Natl. Acad. Sci. U.S.A.* **117**, 17084–17093 (2020).
67. C. R. Marshall, P. D. Ward, Sudden and gradual molluscan extinctions in the latest Cretaceous of Western European Tethys. *Science* **274**, 1360–1363 (1996).
68. B. T. Huber, K. G. MacLeod, R. D. Norris, Abrupt extinction and subsequent reworking of Cretaceous planktonic foraminifera across the Cretaceous-Tertiary boundary: Evidence from the subtropical North Atlantic. *Spec. Pap. Geol. Soc. Am.* **356**, 277–289 (2002).
69. G. Keller, E. Barrera, B. Schmitz, E. Mattson, Gradual mass extinction, species survivorship, and long-term environmental changes across the Cretaceous-Tertiary boundary in high latitudes. *Bull. Geol. Soc. Am.* **105**, 979–997 (1993).
70. T. S. Tobin *et al.*, Extinction patterns, δ18 O trends, and magnetostratigraphy from a southern high-latitude Cretaceous–Paleogene section: Links with Deccan volcanism. *Palaeogeogr. Palaeoclimatol. Palaeoecol.* **350**, 180–188 (2012).
71. T. S. Tobin, Recognition of a likely two phased extinction at the K-Pg boundary in Antarctica. *Sci. Rep.* **7**, 16317 (2017).
72. J. W. Valentine, E. M. Moores, Global tectonics and the fossil record. *J. Geol.* **80**, 167–184 (1972).
73. I. H. Campbell, Large igneous provinces and the mantle plume hypothesis. *Elements* **1**, 265–269 (2005).
74. J. Bezanson, A. Edelman, S. Karpinski, V. B. Shah, Julia: A fresh approach to numerical computing. *SIAM Rev.* **59**, 65–98 (2017).
75. T. Green, P. R. Renne, C. B. Keller, LIP-extinction-correlations. GitHub. https://github.com/Theodore-Green/LIP-Extinction-Correlations. Deposited 10 August 2022.
76. S. Byrne, L. C. Wilcox, V. Churavy, "MPI.jl: Julia bindings for the Message Passing Interface" in *Proceedings of the JuliaCon Conference* (JuliaCon, 2021), vol. 1, p. 68.
77. D. Blackman, S. Vigna, Scrambled linear pseudorandom number generators. arXiv [Preprint] (2018). https://doi.org/10.48550/arXiv.1805.01407 (Accessed 9 March 2022).
78. J. Spray, The Earth Impact Database. http://www.passc.net/EarthImpactDatabase/New%20website_05-2018/Diametersort.html. Accessed 15 July 2022.
79. D. H. Rothman, Carbon-cycle catastrophes: A dynamical-systems perspective. *SIAM News* **52** (2019).
80. S. R. Emerson, J. I. Hedges, *Chemical Oceanography and the Marine Carbon Cycle* (Cambridge University Press, Cambridge, UK, 2008).
81. M. Javoy, F. Pineau, The volatiles record of a "popping" rock from the Mid-Atlantic Ridge at 14 N: Chemical and isotopic composition of gas trapped in the vesicles. *Earth Planet. Sci. Lett.* **107**, 598–611 (1991).
82. Working Group I, "IPCC 2021: Summary for policymakers" in *Climate Change 2021: The Physical Science Basis*, V. Masson-Delmotte *et al.*, Eds. (Cambridge University Press, Cambridge, UK, 2021), pp. 3–32.